

Speeding up Lattice QCD simulations with clover-improved Wilson Fermions

M. Hasenbusch and K. Jansen

*NIC/DESY-Zeuthen
Platanenallee 6, D-15738 Zeuthen, Germany*

e-mail: Martin.Hasenbusch@desy.de, Karl.Jansen@desy.de

Abstract

We apply a recent proposal to speed up the Hybrid-Monte-Carlo simulation of systems with dynamical fermions to two flavour QCD with clover-improvement. The basic idea of our proposal is to split the fermion matrix into two factors with a reduced condition number each. In the effective action, for both factors a pseudo-fermion field is introduced. For our smallest quark masses we see a speed-up of more than a factor of two compared with the standard algorithm.

1 Introduction

It is clear that with simulation algorithms that are used today it will be very difficult, if not impossible, to reach the physical values of lightest quark masses. The scaling behaviour for Wilson fermions (see [1, 2, 3, 4, 5]) of the algorithms predicts enormous costs for simulations at quark masses as light as the u- and d-quarks. To reach this physical point, extrapolations using chiral perturbation theory (χ PT) have to be used. However contact to χ PT seems to be happening at rather small values of the quark masses themselves (see ref. [6] and refs. therein). Any progress to render simulations easier, when approaching the small quark mass regime will help therefore to reach the overlap region between χ PT and lattice QCD allowing for a safe extrapolation to physical quark masses.

Still the HMC (Hybrid-Monte-Carlo) algorithm [7] and its variants [8, 9, 10] are the methods of choice in simulating lattice QCD with dynamical Wilson fermions. Recent large scale simulations with two flavours of Wilson fermions and standard boundary conditions [11, 12] only reach a ratio of $m_\pi/m_\rho \gtrsim 0.58$, while the physical point is given by $m_\pi/m_\rho \approx 0.18$. Note that the decay of the ρ -meson into two π -mesons is only possible if $m_\pi/m_\rho < 0.5$. In refs. [13, 14] explorative studies with $m_\pi/m_\rho \gtrsim 0.4$ were reported and it was found that the simulations become substantially more expensive. Going to light quarks, the HMC algorithm becomes increasingly expensive for at least two reasons: First the condition number of the fermion matrix increases. Hence the number of iterations needed by the solver employed increases. Secondly, but maybe related, the step-size of the integration scheme has to be decreased to maintain a constant acceptance rate. In fact, in ref. [13] a step size as small as 1/400 is needed for the leap-frog integration scheme.

In ref. [15] we have demonstrated that the obstacle of very small step sizes at low values of the quark mass can be lessened by a modification of the pseudo-fermion action. The proposal is to split the fermion matrix into two factors and to introduce a pseudo-fermion field for both factors. Each of the corresponding two matrices has a smaller condition number than the original fermion matrix. As a consequence the “fermion force”, i.e. the response of the system on a variation of the gauge field, is substantially reduced. The numerical study of the two dimensional Schwinger model showed that the step-size can be enlarged and thus the computational effort can be reduced substantially this way. In ref. [16] we presented first results for lattice QCD with two flavours of Wilson fermions and clover improvement [17]. In the present paper we extend this study towards larger lattices and smaller quark masses. Also, we compare two different factorisations of the fermion matrix. We simulated at $\beta = 5.2$ on $8^3 \times 24$ and $16^3 \times 24$ lattices. To allow a comparison with the literature, we have taken the values for the parameters c_{sw} and κ from ref. [18]. Our largest value of κ corresponds to $m_\pi/m_\rho = 0.698$. Results of simulations with Schrödinger functional boundary conditions are reported in ref. [19]. A brief summary of the present work can be

found in [20].

The paper is organised as follows: In section 2 we briefly recall the definition of clover-improved Wilson fermions [17, 21, 22]. As basic improvement we employ even-odd preconditioning as discussed in [23]. Next we discuss in detail the modified pseudo-fermion action [15] and a variant of it [16]. We explain how (easily) the HMC algorithm can be adopted to the modified pseudo-fermion action. It follows a thorough discussion of the integration schemes that we have used. In section 4 we give the details of our simulation. Next we present our numerical results and discuss its implications. Finally we give our conclusions and an outlook.

2 The modified pseudo-fermion action

In this section we remind the reader of the action of clover-improved Wilson fermions. For completeness, we briefly recall even-odd preconditioning and the standard form of the pseudo-fermion action that is used in the HMC simulation. Then we show how the modified pseudo-fermion action that was proposed in ref. [15] can be generalised to clover-improved fermions. In addition to the original proposal, we consider an alternative that is inspired [24] by twisted mass QCD [25] and was first presented in ref. [16]. Finally, we explain how the HMC algorithm can be adopted to the modified pseudo-fermion action.

2.1 The model

Our aim is to simulate the system defined by the partition function

$$Z = \int D[U] \exp(-S_G[U]) \det M[U]^2 \quad , \quad (1)$$

where the Wilson plaquette action is given by

$$S_G[U] = -\frac{\beta}{3} \sum_x \sum_{\mu > \nu} \text{Re Tr} \left(U_{x,\mu} U_{x+\hat{\mu},\nu} U_{x+\hat{\nu},\mu}^\dagger U_{x,\nu}^\dagger \right) \quad , \quad (2)$$

where x are sites on a hyper-cubical lattice, $\mu, \nu \in \{0, 1, 2, 3\}$ are directions on the lattice and $\hat{\mu}$ is a unit vector in μ -direction. In eq. (1), the fermion degrees of freedom have been integrated out. For Wilson fermions with clover-improvement, the fermion matrix M is given by [17]

$$\begin{aligned} M[U]_{xy} &= \left(1 - \frac{i}{2} c_{sw} \kappa \sigma_{\mu\nu} \mathcal{F}_{\mu\nu}(x) \right) \delta_{x,y} \\ &- \kappa \sum_{\mu} \left\{ (1 - \gamma_{\mu}) U_{\mu}(x) \delta_{x+\hat{\mu},y} + (1 + \gamma_{\mu}) U_{\mu}^{\dagger}(x - \hat{\mu}) \delta_{x-\hat{\mu},y} \right\} \quad , \quad (3) \end{aligned}$$

where we sum over μ and ν . The anti-symmetric and anti-Hermitian tensor \mathcal{F} is given by

$$\begin{aligned}
\mathcal{F}_{\mu,\nu} &= \frac{1}{8} [U_\mu(x)U_\nu(x + \hat{\mu})U_\mu^\dagger(x + \hat{\nu})U_\nu^\dagger(x) \\
&+ U_\nu(x)U_\mu^\dagger(x + \hat{\nu} - \hat{\mu})U_\nu^\dagger(x - \hat{\mu})U_\mu(x - \hat{\mu}) \\
&+ U_\mu^\dagger(x - \hat{\mu})U_\nu^\dagger(x - \hat{\nu} - \hat{\mu})U_\mu(x - \hat{\nu} - \hat{\mu})U_\nu(x - \hat{\nu}) \\
&+ U_\nu^\dagger(x - \hat{\nu})U_\mu(x - \hat{\nu})U_\nu(x - \hat{\nu} + \hat{\mu})U_\mu^\dagger(x) \\
&- h.c.] \quad .
\end{aligned} \tag{4}$$

For a discussion of on-shell O(a)-improvement see e.g. refs. [17, 21, 22, 23, 26].

In our simulations we have used even-odd preconditioning throughout. We followed the proposal of ref. [23], see also [27]. The fermion matrix can be written as

$$M = \begin{pmatrix} \mathbb{1}_{ee} + T_{ee} & -\kappa M_{eo} \\ -\kappa M_{oe} & \mathbb{1}_{oo} + T_{oo} \end{pmatrix} \quad , \tag{5}$$

where we have introduced the matrix $T_{ee}(T_{oo})$ on the even (odd) sites as

$$(T)_{xa\alpha,yb\beta} = \frac{i}{2} c_{sw} \kappa \sigma_{\mu\nu}^{\alpha\beta} \mathcal{F}_{\mu\nu}^{ab}(x) \delta_{xy} \quad . \tag{6}$$

The off-diagonal parts M_{eo} and M_{oe} , which connect the even with odd and odd with even lattice sites, respectively, are just the conventional Wilson hopping matrices. The determinant of the fermion matrix can now be written as

$$\det M \propto \det(\mathbb{1}_{ee} + T_{ee}) \det \hat{M} \quad , \tag{7}$$

where

$$\hat{M} = \mathbb{1}_{oo} + T_{oo} - M_{oe}(\mathbb{1}_{ee} + T_{ee})^{-1} M_{eo} \quad . \tag{8}$$

In the following discussion we shall refer to the Hermitian matrix

$$\hat{Q} = \hat{c}_0 \gamma_5 \hat{M} \tag{9}$$

with \hat{c}_0 a constant set to $\hat{c}_0 = 1$ throughout this work.

In the standard HMC simulation of mass-degenerate two-flavour Wilson fermions, the effective action

$$S_{eff}[U, \phi^\dagger, \phi] = S_G[U] + S_{det}[U] + S_F[U, \phi^\dagger, \phi] \quad , \tag{10}$$

with

$$\begin{aligned}
S_{det}[U] &= -2\text{Tr} \log(1 + T_{ee}) \\
S_F[U, \phi^\dagger, \phi] &= \phi^\dagger \hat{Q}^{-2} \phi
\end{aligned} \tag{11}$$

is used. We shall refer to $S_{det}[U]$ as the determinant contribution. The pseudo-fermion action $S_F[U, \phi^\dagger, \phi]$ is based on the representation

$$\det \hat{Q}^2 \propto \int D\phi^\dagger \int D\phi \exp(-\phi^\dagger \hat{Q}^{-2} \phi) \quad (12)$$

of the square of the fermion determinant. In our study we keep $S_G[U]$ and $S_{det}[U]$ in their standard form. However, $S_F[U, \phi^\dagger, \phi]$ is replaced by modified expressions to be discussed below.

As an alternative, the authors of ref. [23] suggest a more symmetrical treatment of even and odd sites. The result is

$$\det M \propto \det(\mathbb{1}_{ee} + T_{ee}) \det(\mathbb{1}_{oo} + T_{oo}) \det \hat{M}_{sym} \quad , \quad (13)$$

where now

$$\hat{M}_{sym} = \mathbb{1}_{oo} - (\mathbb{1}_{oo} + T_{oo})^{-1} M_{oe} (\mathbb{1}_{ee} + T_{ee})^{-1} M_{eo} \quad . \quad (14)$$

The authors of ref. [28] find that the choice of eq. (13) leads to a roughly 30% higher performance of the HMC algorithm than the choice of eq. (7).

Since we wanted to compare our results with those of ref. [18] and we started with our study before ref. [28] appeared, we have used only eq. (7) in this study. However, it is straight-forward to apply our modification to eq. (13) and it can be expected that a similar gain should be found.

2.2 The modified pseudo-fermion action

Our starting point of modifying the action of eq. (11) is the observation that, at fixed acceptance rate and length of the trajectory, the step-size of the integration scheme has to be decreased with decreasing sea-quark masses and hence with increasing condition number of the fermion matrix. This effect can be nicely seen e.g. in table II of ref. [11].

Also, a number of studies (see e.g. [29, 30, 31]) have shown that replacing the original fermion matrix by a preconditioned fermion matrix in the pseudo-fermion action allows for a larger step-size in the HMC simulation at the same acceptance rate.

Based on these observations, one of us [15] proposed to factorise the fermion matrix into two parts, with reduced condition number each. The determinant of both factors is estimated by pseudo-fermion fields: ¹

$$\begin{aligned} \det \hat{Q}^2 &= \det W W^\dagger \det [W^{-1} \hat{Q}] [W^{-1} \hat{Q}]^\dagger \propto \int D\phi_1^\dagger \int D\phi_1 \int D\phi_2^\dagger \int D\phi_2 \\ &\quad \exp \left(-\phi_1^\dagger (W W^\dagger)^{-1} \phi_1 - \phi_2^\dagger \left([W^{-1} \hat{Q}] [W^{-1} \hat{Q}]^\dagger \right)^{-1} \phi_2 \right) \quad . \quad (15) \end{aligned}$$

¹In refs. [30, 32] we applied a similar modification of the pseudo-fermion action to speed up the local updating of lattice QCD.

Note that W might be non-Hermitian. In the following we shall use the notation

$$S_{F1} = \phi_1^\dagger (WW^\dagger)^{-1} \phi_1 \quad , \quad S_{F2} = \phi_2^\dagger \left([W^{-1}\hat{Q}][W^{-1}\hat{Q}]^\dagger \right)^{-1} \phi_2 \quad . \quad (16)$$

In ref. [15] we also considered even-odd preconditioning, but no clover-improvement. We constructed W by a shift in the hopping-parameter κ : $W = \gamma_5 \tilde{M}$, where

$$\tilde{M} = \mathbb{1} - \tilde{\kappa}^2 M_{oe} M_{eo} \quad , \quad (17)$$

with $\tilde{\kappa} < \kappa$. Since the fermion matrix can be multiplied by a constant factor without changing the physics, we can write equivalently

$$W = \hat{Q} + \rho\gamma_5 \quad . \quad (18)$$

This is the form that we apply to the even-odd preconditioned, clover-improved \hat{Q} of eq. (9). In ref. [15] we have demonstrated at the example of the two-dimensional Schwinger model that the step-size of the integration scheme can indeed be increased compared with the standard pseudo-fermion action. This gain increases as the sea-quark mass decreases. For the lightest mass that we studied, the step-size could be increased by more than a factor of two for the optimal choice of $\tilde{\kappa}$.

In addition to the original choice (18) of W we shall consider

$$\tilde{W} = \hat{Q} + i\rho\mathbb{1} \quad , \quad (19)$$

which is inspired [24] by twisted mass QCD [25] and was first tested in ref. [16].

In terms of \hat{Q} the resulting pseudo-fermion action is $S_F = S_{F1} + S_{F2}$ with

$$S_{F1} = \phi_1^\dagger [\hat{Q} + \rho\gamma_5]^{-2} \phi_1 \quad , \quad S_{F2} = \phi_2^\dagger [\mathbb{1} + \rho\gamma_5\hat{Q}^{-1}][\mathbb{1} + \rho\hat{Q}^{-1}\gamma_5] \phi_2 \quad (20)$$

for eq. (18) and $\tilde{S}_F = \tilde{S}_{F1} + \tilde{S}_{F2}$ with

$$\tilde{S}_{F1} = \phi_1^\dagger [\hat{Q}^2 + \rho^2\mathbb{1}]^{-1} \phi_1 \quad , \quad \tilde{S}_{F2} = \phi_2^\dagger [\mathbb{1} + \rho^2\hat{Q}^{-2}] \phi_2 \quad (21)$$

for eq. (19).

The aim of our modification is to use matrices with reduced condition number in the pseudo-fermion action. Let us denote the smallest and the largest eigenvalue of \hat{Q}^2 by λ_{min} and λ_{max} , respectively. If we choose $\lambda_{min} \ll \rho^2 \ll \lambda_{max}$, we find the condition number of $\hat{Q}^2 + \rho^2$ to be λ_{max}/ρ^2 . On the other hand, the condition number of the second matrix used in \tilde{S}_{F2} of eq. (21) becomes ρ^2/λ_{min} . This suggests an optimal choice of ²

$$\rho^2 = \sqrt{\lambda_{max}\lambda_{min}} \quad . \quad (22)$$

²We are grateful to R. Sommer for this argument.

In the simulations with the pseudo-fermions using the action \tilde{S}_F of eq. (21), as described below, we followed this rule. The obvious disadvantage of this choice is that the eigenvalues λ_{min} and λ_{max} have to be computed to a reasonable accuracy before the simulation with the modified pseudo-fermions can be done with optimised choices of the algorithm. Also it is not clear, how much the detailed distribution of the eigenvalues of \hat{Q}^2 matters for the step size of the integration scheme used.

Therefore we did not use the rule of eq. (22) in the simulations with the action of eq. (20). Instead, we tried to find numerically the value of ρ , where for fixed step-size the acceptance rate is the largest.

As a last remark in this section we want to mention that with the choice of ρ^2 of eq. (22) it seems that the condition number k of the original action, eq. (11), is reduced to \sqrt{k} when using the action given in eq. (21). If hence the scaling behaviour of the HMC algorithm is indeed determined to a large extend by the condition number of the fermion matrix used, a much better scaling behaviour can be expected when the chiral limit is approached.

2.3 The Hybrid-Monte-Carlo Algorithm

For completeness, we recall the steps of the Hybrid-Monte-Carlo algorithm [7] applied to the standard pseudo-fermion action of eq. (10). One elementary update (“trajectory”) of the HMC algorithm is composed of the following steps:

- Global heat-bath of the pseudo-fermions and the conjugate momenta.
- Molecular dynamics evolution of the gauge-field and the conjugate momenta P with fixed pseudo-fermions.
- Accept/Reject step: the gauge-field U' that is generated by the molecular dynamics evolution is accepted with the probability $P_{acc} = \min[1, \exp(-H(U', P', \phi) + H(U, P, \phi))]$, where P' represents the conjugate momenta generated in the molecular dynamics evolution.

The last step is needed, as the molecular dynamics evolution can not be done exactly and hence requires a numerical integration scheme, rendering $\Delta H = H(U, P, \phi) - H(U', P', \phi) \neq 0$. To obtain a valid algorithm, this scheme has to be area preserving and reversible. Details on the numerical integration schemes that we have studied are given in section 3.

2.4 Heat-bath of the pseudo-fermion fields

The field ϕ_1 is initialised at the beginning of the trajectory as usual³:

$$\phi_1 = W \eta_1 \quad , \quad (23)$$

where η_1 has a Gaussian distribution. The heat-bath of ϕ_2 however requires the application of the inverse of W :

$$\phi_2 = W^{-1} \hat{Q} \eta_2 \quad , \quad (24)$$

where also η_2 has a Gaussian distribution.

2.5 The variation of the pseudo-fermion action

An important feature of our approach is that the variation of the modified pseudo-fermion action can be computed as easily as in the standard case. For the first part of the pseudo-fermion action we obtain upon a variation of the action with respect to the gauge fields

$$\delta S_{F1} = -X^\dagger \delta W Y - Y^\dagger \delta W^\dagger X \quad (25)$$

with the vectors

$$X = (WW^\dagger)^{-1} \phi_1 \quad , \quad Y = W^{-1} \phi_1 \quad , \quad (26)$$

which is essentially the same as for the standard pseudo-fermion action. The only difference is that \hat{Q} is replaced by W .

For the second part of the pseudo-fermion action we get

$$\delta S_{F2} = -X^\dagger \delta \hat{Q} Y - Y^\dagger \delta \hat{Q}^\dagger X + X^\dagger \delta W \phi_2 + \phi_2^\dagger \delta W^\dagger X \quad (27)$$

with the vectors

$$X = \left(\hat{Q} \right)^{-2} W \phi_2 \quad , \quad Y = \hat{Q}^{-1} W \phi_2 \quad . \quad (28)$$

For our choices of W in eq. (18) (and of \tilde{W} in eq. (19)) the variation of S_{F2} (and \tilde{S}_{F2}) further simplifies and it holds $\delta W = \delta \hat{Q}$ ($= \delta \tilde{W}$). We therefore get

$$\delta S_{F2} = -X^\dagger \delta \hat{Q} Y - Y^\dagger \delta \hat{Q} X \quad , \quad (29)$$

where

$$X = \hat{Q}^{-1} [\mathbb{1} + \rho \hat{Q}^{-1} \gamma_5] \phi_2 \quad , \quad Y = \rho \hat{Q}^{-1} \gamma_5 \phi_2 \quad (30)$$

³Here we discuss only the case of the action S_F in eq. (20). The case of the action \tilde{S}_F in eq. (21) is basically identical.

for the action in eq. (20) and

$$X = \rho^2 \hat{Q}^{-2} \phi_2 \quad , \quad Y = \hat{Q}^{-1} \phi_2 \quad (31)$$

for the action in eq. (21).

Let us discuss the effect of introducing the parameter ρ^2 on the variation of the pseudo-fermion actions. Since the step size used in the HMC algorithm increases as the condition number decreases, we expect that we can choose a larger step size for the action \tilde{S}_{F1} . For the action \tilde{S}_{F2} we see from eq. (31) that its variation includes a factor of ρ^2 . Since $\rho^2 \ll 1$, we expect again smaller variations of the action along a trajectory leading to larger choices of the step size. A similar argument holds for the action S_F of eq. (20).

3 Integration schemes

We have tested two different integration schemes: The standard leap-frog and a partially improved one suggested by Sexton and Weingarten (see eq. (6.4) of ref. [33]) that still has an $\delta\tau^2$ error as the leap-frog scheme. However the amplitude of this error is considerably reduced.

Let us define the update of the gauge-field and the momenta as

$$T_U(\delta\tau) \quad : \quad U \rightarrow e^{i\delta\tau P} U \quad (32)$$

$$T_P(\delta\tau) \quad : \quad P \rightarrow P - i\delta\tau \delta_U(S_g(U) + S_f(U)) \quad , \quad (33)$$

where δ_U denotes a variation with respect to the gauge fields.

The elementary step of the leap-frog algorithm is given by

$$T_2(\delta\tau) = T_P\left(\frac{\delta\tau}{2}\right) T_U(\delta\tau) T_P\left(\frac{\delta\tau}{2}\right) \quad . \quad (34)$$

A trajectory is composed of N_{md} consecutive elementary steps. Here we use trajectories of length 1, i.e. $N_{md} \delta\tau = 1$, as it is done in most HMC simulations. Note that the order of the updates of momenta and gauge-fields is not unique. In fact, in ref. [28] it was demonstrated that the alternative order

$$T'_2(\delta\tau) = T_U\left(\frac{\delta\tau}{2}\right) T_P(\delta\tau) T_U\left(\frac{\delta\tau}{2}\right) \quad (35)$$

achieves the same acceptance rate as eq. (34) (see fig. 2 of ref. [28]) with a roughly 15% larger step size $\delta\tau$.

Since we like to compare our numerical results with those of ref. [18] we have used the order of eq. (34) in our numerical study. Also it is not clear to us how the idea of a split time-scale introduced in ref. [33] can be applied to eq. (35).

In the literature [33, 34, 35] also higher-order schemes are discussed. These schemes become increasingly complicated as the order increases. Recent studies

[11, 36, 37] show that higher-order schemes become less efficient than the simple leap-frog integration scheme of eq. (34) as κ_c is approached.

In addition to the genuinely higher-order schemes, Sexton and Weingarten [33] discuss a scheme with reduced $\delta\tau^2$ errors. In the numerical tests, using Wilson fermions, on a 4^4 lattice at $\beta = 5.4$ and $\kappa = 0.162$, Sexton and Weingarten [33] found that this scheme achieves the best performance. The elementary step of this scheme is given by

$$T_4(\delta\tau) = T_P\left(\frac{\delta\tau}{6}\right) T_U\left(\frac{\delta\tau}{2}\right) T_P\left(\frac{2}{3}\delta\tau\right) T_U\left(\frac{\delta\tau}{2}\right) T_P\left(\frac{\delta\tau}{6}\right) . \quad (36)$$

Note that in an elementary step of this scheme, the variation of the action with respect to the gauge-fields has to be computed twice. Comparing the efficiency of this scheme and the leap-frog we have to keep this factor of two in mind.

In our study we are primarily interested in the effect of the pseudo-fermions on the step-size of the integration scheme. Therefore we have employed the split of the time-scale proposed by Sexton and Weingarten [33]. This, in practice, allows to eliminate completely the effect of the gauge action on the step-size.

The update of the momenta is split into two parts: One with respect to the gauge action and one with respect to the pseudo-fermion action:

$$T_{PG}(\delta\tau) \quad : \quad P \rightarrow P - i\delta\tau \delta_U S_g(U) \quad (37)$$

$$T_{PF}(\delta\tau) \quad : \quad P \rightarrow P - i\delta\tau \delta_U S_f(U) . \quad (38)$$

The leap-frog scheme is now generalised to

$$T_2(n, \delta\tau) = T_{PF}\left(\frac{\delta\tau}{2}\right) \left[T_{PG}\left(\frac{\delta\tau}{2n}\right) T_U\left(\frac{\delta\tau}{n}\right) T_{PG}\left(\frac{\delta\tau}{2n}\right) \right]^n T_{PF}\left(\frac{\delta\tau}{2}\right) . \quad (39)$$

The improved scheme in eq. (36) is generalised to

$$T_4(n, \delta\tau) = T_{PF}\left(\frac{\delta\tau}{6}\right) X\left(\frac{\delta\tau}{2}\right) T_{PF}\left(\frac{2}{3}\delta\tau\right) X\left(\frac{\delta\tau}{2}\right) T_{PF}\left(\frac{\delta\tau}{6}\right) , \quad (40)$$

where

$$X(\delta\tau) = T_{PG}\left(\frac{\delta\tau}{6}\right) T_U\left(\frac{\delta\tau}{2}\right) T_{PG}\left(\frac{2}{3}\delta\tau\right) T_U\left(\frac{\delta\tau}{2}\right) T_{PG}\left(\frac{\delta\tau}{6}\right) . \quad (41)$$

In our study we have used $n = 4$ throughout. We have tested that larger values of n hardly further increase the acceptance rates.

4 The Numerical Study

We have tested our modified algorithm at parameters that had been studied by UKQCD before [18]. We have performed simulations at $\beta = 5.2$ and $c_{sw} = 1.76$.

Note that $c_{sw} = 1.76$ was a preliminary result for the improvement coefficient, while the final analysis resulted in $c_{sw} = 2.0171$ for $\beta = 5.2$ [22]. We applied periodic boundary conditions in all lattice directions, except for anti-periodic boundary conditions in time-direction for the fermion-fields.

As a first step we have studied a $8^3 \times 24$ lattice at $\kappa = 0.137$. Later we simulated a $16^3 \times 24$ lattice at $\kappa = 0.139, 0.1395$ and 0.1398 . Following the tables 4.4 and 4.6 of ref. [18], these values of κ correspond to $m_\pi/m_\rho \approx 0.856, 0.792, 0.715$ and 0.686 , respectively. From table 4.8 of ref. [18] we read that $\kappa_c \approx 0.1405$ with an error of about one in the last digit.

4.1 Details of the implementation

We have simulated the two modified actions with independent programs. The program for the action \tilde{S}_F in eq. (21) was written in TAO and was executed on a APE100 computer. The program for the action S_F in eq. (20) was written in C with sequences of assembler code to take advantage of the SSE2-instructions of the Pentium 4 CPU (See ref. [38]). Since the implementation in the two cases differ in many respects, we give separate discussions of the details below.

4.1.1 The action S_F

Here we have used double-precision floating point arithmetic throughout. We have implemented the BiCGstab algorithm [39] to solve the linear equations (24,26,30) and to compute the action at the end of the trajectory.

As start vector we have always used the zero-vector. The square of the residual is given by

$$r^2 = |M\eta^{(m)} - \phi|^2 \quad , \quad (42)$$

where $\eta^{(m)}$ is the approximation of the solution after the m^{th} iteration. Note that we did not compute r^2 using eq. (42) directly, but used instead the iterated result of the BiCGstab algorithm. The iteration is stopped after r^2 becomes smaller than a given bound. For the heat bath of eq. (24) of the field ϕ_2 and to compute the action at the end of the trajectory we have required $r^2 < 10^{-20}$.

As long as the start vector does not depend on the history of the trajectory, the correctness of the HMC algorithm does not rely on the accuracy of the vectors X and Y of section 2.5. However, if the accuracy becomes too low, ΔH becomes large and hence the acceptance rate low.

The vectors X and Y for S_{F1} we computed as follows:

$$\tilde{M}Y = \gamma_5\phi_1 \quad , \quad (43)$$

where we required

$$r^2 < 0.01R^2 \quad (44)$$

as stopping criterion, where R^2 is a certain cut-off, the choices of which are listed below. For the solution X of

$$\tilde{M}X = \gamma_5 Y \quad (45)$$

we required $r^2 < R^2$. Here we followed the recommendation of ref. [18]. Since the error of Y propagates to X , we can not reach the same accuracy of X as of Y . Therefore it is reasonable to require a higher accuracy for eq. (43) than for eq. (45).

In a similar fashion we compute the vectors X and Y for the second part of the pseudo-fermion action S_{F2} :

$$\hat{M}Y = \rho\phi_2 \quad , \quad (46)$$

where we require $r^2 < 0.01R^2$. The vector X is then obtained through

$$\tilde{M}X = \gamma_5(\phi_2 + Y) \quad , \quad (47)$$

with the stopping criterion $r^2 < R^2$.

Unfortunately, there is also a subtle effect of the accuracy of X and Y on the reversibility of the algorithm. For a discussion see refs. [28, 40, 41, 42] and refs. quoted therein. We performed a few checks to investigate this problem. We find that the amplitude of the reversibility violations is much the same for the leap-frog as for the Sexton-Weingarten improved scheme. Also it does not depend much on the parameter ρ of the modified pseudo-fermion action. On the other hand we see, in accordance with the literature, that the reversibility violations become much worse when we compute X and Y with reduced accuracy. Going a trajectory of length 1 forward and backward again, we see for $\kappa = 0.1398$ violations in the Hamiltonian that are smaller than 10^{-8} for $R^2 = 10^{-20}$. On the other hand, for $R^2 = 10^{-4}$ the violations become as large as 10^{-2} . Nevertheless, these reversibility violations are still small enough, not to invalidate the results reported below.

In the case that the BiCGstab algorithm fails to converge, which never happened in our study, X and Y have to be computed with the conjugate gradient algorithm:

For S_{F1} we first compute X as the solution of

$$W^2X = \phi_1 \quad (48)$$

followed by

$$Y = WX \quad . \quad (49)$$

For S_{F2} we first compute X as the solution of

$$\hat{Q}^2X = (\hat{Q} + \rho\gamma_5)\phi_2 \quad (50)$$

followed by

$$Y = \hat{Q}X - \phi_2 \quad . \quad (51)$$

4.1.2 The action \tilde{S}_F

These simulations were performed with single precision arithmetic throughout. As solver we have used the conjugate gradient algorithm. As start vector we have used the solution of the previous step. The vectors X and Y for \tilde{S}_{F1} are computed as follows: First we solve the linear equation

$$[\hat{Q}^2 + \rho^2]X = \phi_1 \quad (52)$$

followed by

$$Y = \tilde{W}^\dagger X \quad (53)$$

For \tilde{S}_{F2} we solve

$$\hat{Q}^2 X = \rho^2 \phi_1 \quad (54)$$

followed by

$$Y = \rho^{-2} \tilde{W}^\dagger X \quad (55)$$

For X we tried to reach essentially the machine precision. Thus, as stopping criterion we required that the square of the iterated residual divided by the square of the norm of X is smaller than 10^{-8} .

4.2 Analysing the Performance of the Algorithm

The goal of the optimisation of an algorithm is to obtain a given statistical error for the observable one wants to compute with a minimal amount of CPU time. To this end, the ALPHA-collaboration has studied in a benchmark of various algorithms [30] the quantity

$$M_{cost} = \frac{\text{CPU-time}}{(\text{stat. error})^2} \quad (56)$$

The practical problem with this definition is that it requires rather large statistics to obtain reliable results for the integrated auto-correlation time τ_{int} and correspondingly for the statistical error. On the other hand it requires only a rather small number (say 100) of trajectories to obtain an accurate estimate of the acceptance rate. Therefore we shall base our study on the hypothesis that for a fixed length of the trajectory and a fixed acceptance rate, the auto-correlation times are independent on the parameter ρ of the modified pseudo-fermion action and the integration scheme that is used. In fact, this hypothesis is backed up by the simulations of the Schwinger model in ref. [15] and the simulations of the $8^3 \times 24$ lattice presented below.

Following this hypothesis, we are looking for the parameter ρ that allows for the largest step-size (i.e. minimal CPU-cost) at a given acceptance rate. This requires however fine tuning of $\delta\tau$ for each parameter of ρ . Instead we have kept the step-size $\delta\tau$ fixed and have searched for the value of ρ with the maximal

acceptance rate. The number of iterations needed to solve the linear equations, given in eq. (26), depends on ρ . On the other hand the linear equations, given in eq. (28), always involve the matrix \hat{Q} and hence the number of iterations does not depend on ρ . Since the number of iterations for eq. (28) is, at least for $\kappa \rightarrow \kappa_c$, much larger than that for equations eq. (26) we shall ignore the dependence of the total iteration number on ρ and concentrate on the acceptance rate.

4.3 Simulation results

4.3.1 Simulations of the $8^3 \times 24$ lattice

As a first step, we have studied quite extensively the $8^3 \times 24$ lattice at $\kappa = 0.137$. First we searched for the optimal value of ρ for the action S_F in eq. (20). After thermalising the system, we performed runs with 200 trajectories each for a range of values for ρ . We have fixed the step size $\delta\tau = 0.02$ for the leap-frog scheme and $\delta\tau = 0.05$ for the Sexton-Weingarten improved scheme. The results for the acceptance rate are summarised in figure 1. In order to determine the acceptance rate, we have averaged $\min[1, \exp(-\Delta H)]$ instead of counting the accepted configurations. In this way the statistical error of the acceptance rate is considerably reduced.

We first observe that the acceptance rate with the modified pseudo-fermion action is indeed higher than for the standard action ($\rho = 0$). For both integration schemes we see a rather broad maximum of the acceptance rates and the maximal acceptance is reached for $\rho \approx 0.5$.

In order to compare the efficiency of the various approaches, we have performed more extended runs for $\rho = 0$ and $\rho = 0.5$ with the action S_F , eq. (20), and for the action \tilde{S}_F , eq. (21). In the case of \tilde{S}_F we have chosen ρ following the rule given in eq. (22). In these extended runs we have chosen the step-size $\delta\tau$ such that $P_{acc} \approx 0.8$. The parameters of these runs and the acceptance rates are summarised in table 1. In the case of the leap-frog scheme the step-size can be increased by a factor of about 1.6 by using the modified pseudo-fermion action S_F , eq. (20). In the case of the Sexton-Weingarten improved scheme, we see a similar increase of the step-size by a factor of approximately 1.7. The pseudo-fermion action S_F seems to perform slightly better than the action \tilde{S}_F . Comparing the leap-frog and the Sexton-Weingarten improved scheme, we see a small advantage for the Sexton-Weingarten improved scheme, independent of the pseudo-fermion action that is used.

In table 2 we give our results for the plaquette and the minimal and maximal eigenvalue of \hat{Q}^2 for the runs with the action S_F of eq. (20). The observed consistency of the results for these observables among the three runs gives us confidence that the modified pseudo-fermion action has been correctly implemented in the program. Also the result $P = 0.49405(34)$ for the plaquette given in ref. [18] is in reasonable agreement with ours. From the run with the action \tilde{S}_F we get

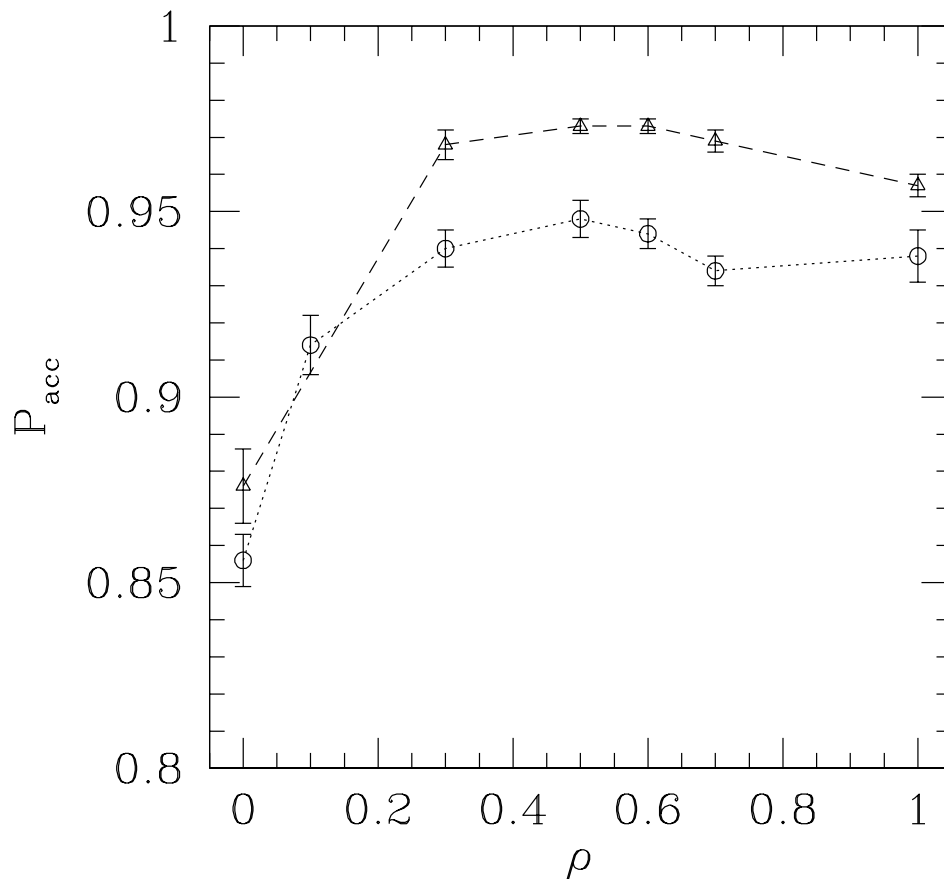


Figure 1: Results for the acceptance rate of the leap-frog scheme (circle) and the Sexton-Weingarten improved scheme (triangle) as function of the parameter ρ . The dashed and the dotted lines should only guide the eye. For the leap-frog scheme, we have fixed the step-size to $\delta\tau = 0.02$ and for the Sexton-Weingarten improved scheme to $\delta\tau = 0.05$. The simulations are performed on a $8^3 \times 24$ lattice at $\beta = 5.2$, $c_{sw} = 1.76$ and $\kappa = 0.137$. The pseudo-fermion action S_F of eq. (20) is used.

$\lambda_{min} = 0.00584(4)$, which is also consistent with the results obtained with the action S_F .

For the runs with the action S_F , eq. (20), we have computed integrated auto-correlation times for the plaquette and for λ_{min} . We have truncated the summation of the auto-correlation function at $t = 80$. Within error-bars the integrated autocorrelation times are the same for the three runs. I.e. our hypothesis that the autocorrelation times do not depend very much on the integration scheme and the form of the pseudo-fermion action, as long as the acceptance rate is the same, is confirmed.

In table 3 we give the iteration numbers that are needed by the BiCGstab solver in the simulations with the action S_F . We will denote by N_1 the number of iterations for the action S_{F1} (\tilde{S}_{F1}) and with N_2 the number of iterations for the action S_{F2} (\tilde{S}_{F2}). N_1 constitutes the numerical overhead caused by the extra part S_{F1} (\tilde{S}_{F1}) of the modified pseudo-fermion action. As can be seen in table 3, N_2 depends only little on ρ , as expected, since here the original matrix \hat{Q}^2 has to be inverted. Since most of the CPU-time is spent for the solver, the total number of solver-iterations per trajectory is a good indicator for the numerical effort.

We see that, despite the numerical overhead due to the additional pseudo-fermion field, a net advantage for the modified pseudo-fermion action remains, as demonstrated by the total number of iterations given in the last column in table 3. As we shall see below, this total number of iterations can be further reduced by choosing a larger value of R^2 , see eq. (44). However, this affects the simulation of the standard pseudo-fermion action and the modified pseudo-fermion action in the same way. Hence our conclusion on the relative performance gain is not affected.

In the simulation of the pseudo-fermion action \tilde{S}_F we find the average iteration numbers of the conjugate gradient solver to be $N_2 = 121.8(3)$ at $\rho = 0$ and $N_1 = 27.278(3)$ and $N_2 = 122.1(3)$ for $\rho = 0.348$. Note that here we have used the same stopping criterion for the calculation of the “force” as for the calculation of the action at the end of the trajectory. Again N_2 does not depend on ρ and N_1 gives the overhead of the simulation with the modified pseudo-fermion action. It is difficult to compare the iteration numbers of the CG and the BiCGstab in our study, since different stopping criteria have been used. Nevertheless, if we compare twice the iteration number of the BiCGstab with the iteration number of the CG, as we should, we end up with a ratio of $N_2^{CG}/(2\tilde{N}_2^{BiCG}) \approx 1.75$. Choosing more comparable stopping criteria, as was done in ref. [18], an advantage of 40% in favour of the BiCGstab solver can be found. Note however that the BiCGstab requires more linear algebra operations per iteration than the CG. E.g. on the APE100 computer this means that the BiCGstab and the CG solver require approximately the same CPU-time.

Next we tested what accuracy of the solver is needed in the calculation of the variation of the action to maintain a high acceptance rate. For this purpose we have performed runs with 200 trajectories each for the action S_F with $\rho = 0$

Table 1: Results for extended runs for the $8^3 \times 24$ lattice with $\beta = 5.2$, $\kappa = 0.137$ and $c_{sw} = 1.76$. We have used either the leap-frog (L) or the Sexton-Weingarten improved (S) scheme; "stat" gives the number of trajectories that have been generated. P_{acc} is the acceptance rate. In the runs with the pseudo-fermion action S_F , eq. (20), we have averaged $\min[1, \exp(-\Delta H)]$. In the case of \tilde{S}_F , eq. (21), we have just counted the accepted configurations.

scheme	action	ρ	$\delta\tau$	stat	P_{acc}
L	eq. (20)	0.0	0.025	6030	0.793(3)
L	eq. (20)	0.5	0.04	8300	0.770(3)
S	eq. (20)	0.5	0.1	6170	0.883(2)
S	eq. (21)	0.0	0.06	2400	0.83(1)
S	eq. (21)	0.348...	0.1	8000	0.798(9)

Table 2: Observables for the runs with the action of S_F , eq. (20), of the previous table. P is the value of the plaquette. λ_{min} and λ_{max} are the minimal and maximal eigenvalue of \hat{Q}^2 . Computing τ_{int} for the plaquette and λ_{min} we summed autocorrelation-functions up to $t = 80$.

scheme	ρ	P	$\tau_{int,P}$	λ_{min}	$\tau_{int,\lambda}$	λ_{max}
L	0.0	0.49474(29)	25.8(6.0)	0.00593(4)	9.3(2.2)	2.8377(11)
L	0.5	0.49487(22)	23.2(4.6)	0.00591(3)	8.2(1.6)	2.8381(9)
S	0.5	0.49457(27)	24.4(5.6)	0.00596(4)	9.6(2.2)	2.8389(10)

Table 3: Iterations needed by the BiCGstab solver. N_1^{acc} and N_2^{acc} are the numbers of iterations that were needed to compute S_{F1} and S_{F2} of eq. (20), respectively, at the end of the trajectory. N_1^{traj} and N_2^{traj} are the iteration numbers that are needed to compute the vectors Y for S_{F1} and S_{F2} of eq. (20), respectively. N^{total} is the total number of iterations needed for one trajectory. τ_N is the auto-correlation time of the total number of iterations.

scheme	ρ	N_1^{acc}	N_2^{acc}	N_1^{traj}	N_2^{traj}	τ_N	N^{total}
L	0.0	-	60.4(2)	-	34.11(11)	21.1(4.9)	2777(9)
L	0.5	18.762(8)	61.2(2)	11.533(7)	34.89(9)	19.4(3.9)	2362(5)
S	0.5	18.750(13)	60.9(2)	11.527(8)	34.78(12)	23.1(5.3)	1922(5)

Table 4: *Runs with 200 trajectories each for the $8^3 \times 24$ lattice, $\beta = 5.2$, $c_{sw} = 1.76$ and $\kappa = 0.137$. The pseudo-fermion action of eq. (20) is used. Here we study the dependence of the acceptance rate P_{acc} on the stopping criterion R^2 of the BiCGstab solver, see eq. (44).*

scheme	ρ	$\delta\tau$	R^2	P_{acc}	N^{total}
L	0.0	0.025	1	0.410(27)	1022(6)
L	0.0	0.025	0.1	0.723(20)	1230(5)
L	0.0	0.025	0.01	0.809(17)	1430(6)
L	0.5	0.04	1	0.390(26)	941(5)
L	0.5	0.04	0.1	0.687(22)	1078(5)
L	0.5	0.04	0.01	0.741(18)	1269(6)
S	0.5	0.1	1	0.361(26)	782(3)
S	0.5	0.1	0.1	0.747(19)	899(5)
S	0.5	0.1	0.01	0.863(11)	1030(4)

and $\rho = 0.5$ and the same step-sizes as for the runs reported in the table 1 and various values for R^2 . Our results are summarised in table 4. We observe that the dependence of the acceptance rate on R^2 is much the same for $\rho = 0$ and for $\rho = 0.5$ as well as for the two choices of the integration scheme. Going from $R^2 = 0.1$ to $R^2 = 1$, the acceptance rate drastically drops. On the other hand, for $R^2 = 0.01$ we have essentially reached the acceptance rate of $R^2 = 10^{-8}$ that is given in table 1.

4.3.2 Simulations of the $16^3 \times 24$ lattice

In order to have a more difficult situation, we went on to the $16^3 \times 24$ lattice with κ -values that are closer to κ_c . In particular, we have performed simulations at $\kappa = 0.1390, 0.1395$ and 0.1398 with the pseudo-fermion action S_F of eq. (20). For comparison, we have also simulated the action \tilde{S}_F of eq. (21) at $\kappa = 0.1395$.

Our results for the acceptance rate and the total number of iterations of the BiCGstab solver per trajectory for $\kappa = 0.1390$ and 0.1398 are summarised in table 5. For each set of parameters we have generated 100 trajectories, starting from an equilibrated configuration. Since the integrated auto-correlation time of the acceptance rate is very small, we can give meaningful error-estimates for this quantity. On the other hand, as we have learned from the longer runs of the $8^3 \times 24$ lattice, the integrated auto-correlation time of the total number of iterations is much larger. Hence we do not quote error-bars for N^{total} and consider N^{total} to give only an indication for the relative CPU-costs of the simulations.

Let us start the discussion by testing the effect of the stopping criterion R^2 of the BiCGstab solver on the acceptance rate. For the leap-frog scheme with

$\rho = 0.5$ and $\kappa = 0.1390$ the acceptance rate for $R^2 = 0.01$ is almost the same as for $R^2 = 0.001$, while it drastically drops as we further relax the stopping criterion to $R^2 = 0.1$ and $R^2 = 1.0$. In order to keep the effect of R^2 on the acceptance rate small we have chosen $R^2 = 0.001$ or $R^2 = 0.0001$ in the following simulations for $\kappa = 0.139$. In the case of $\kappa = 0.1398$ we see a similar dependence of the acceptance on R^2 . Here we have chosen $R^2 = 0.0001$ for most of the simulations.

Next, we studied the dependence of the acceptance rate on the parameter ρ of the modified pseudo-fermion action. For the leap-frog scheme with $\rho \neq 0$ we have used the step-size $\delta\tau = 0.02$. As can be seen in table 5, the maximum of the acceptance rate is reached at $\rho = 0.5$ for $\kappa = 0.1390$ as well as $\kappa = 0.1398$. As for the $8^3 \times 24$ lattice at $\kappa = 0.137$, this maximum is broad. This means that no fine tuning is needed to obtain almost optimal performance. In order to obtain the same acceptance rate for $\rho = 0$ as for $\rho = 0.5$ the step-size has to be halved. The performance of the algorithm in terms of N^{total} using S_F is shown in fig. 2. We selected points from table 5 that have an acceptance rate of about 80%. For the case of the leap-frog integrator we find a gain in performance by a factor of 1.66 at $\kappa = 0.1390$, which becomes 1.79 at $\kappa = 0.1398$ compared with the standard pseudo-fermion action.

It is interesting to note that in contrast to our discussion in section 4.2 the optimal value of ρ is the same for $\kappa = 0.1390$ and $\kappa = 0.1398$. One explanation might be that the low eigenmodes of the fermion matrix become relevant for the dynamics of the HMC algorithm with the leap-frog scheme only for κ even closer to κ_c .

For the case of the Sexton-Weingarten improved scheme, we find, at $\kappa = 0.1398$, a gain of a factor of 2.4 in favour of the modified pseudo-fermion action. It is also interesting to note from table 5 that in this case the optimal value of ρ decreases as κ approaches κ_c , following our expectations. The difference in the behaviour of the optimal values of ρ between the two integration schemes is not too surprising. For the standard pseudo-fermion action the step-size of higher order integration schemes has to be reduced more drastically than for the leap-frog scheme (see e.g. ref. [36]).

For $\rho = 0$ at $\kappa = 0.1398$ we obtain an acceptance rate of 82% with the Sexton-Weingarten improved scheme and $\delta\tau = 0.0166\dots$. This means that for the standard pseudo-fermion action, the Sexton-Weingarten improved scheme performs worse than the leap-frog scheme. On the other hand, the gain due to the modified pseudo-fermion action is much larger for the Sexton-Weingarten improved scheme than for the leap-frog scheme which explains the gain in performance shown in fig. 2.

In table 6 we give results for $\kappa = 0.1395$ for both pseudo-fermion actions of S_F and \tilde{S}_F . Here we have only used the Sexton-Weingarten improved scheme. The acceptance rate as well as the step-size for S_F are slightly larger than for \tilde{S}_F . Comparing the two modified pseudo-fermion actions we find hence a minor advantage for S_F . Clearly, more studies have to be performed to be able to make

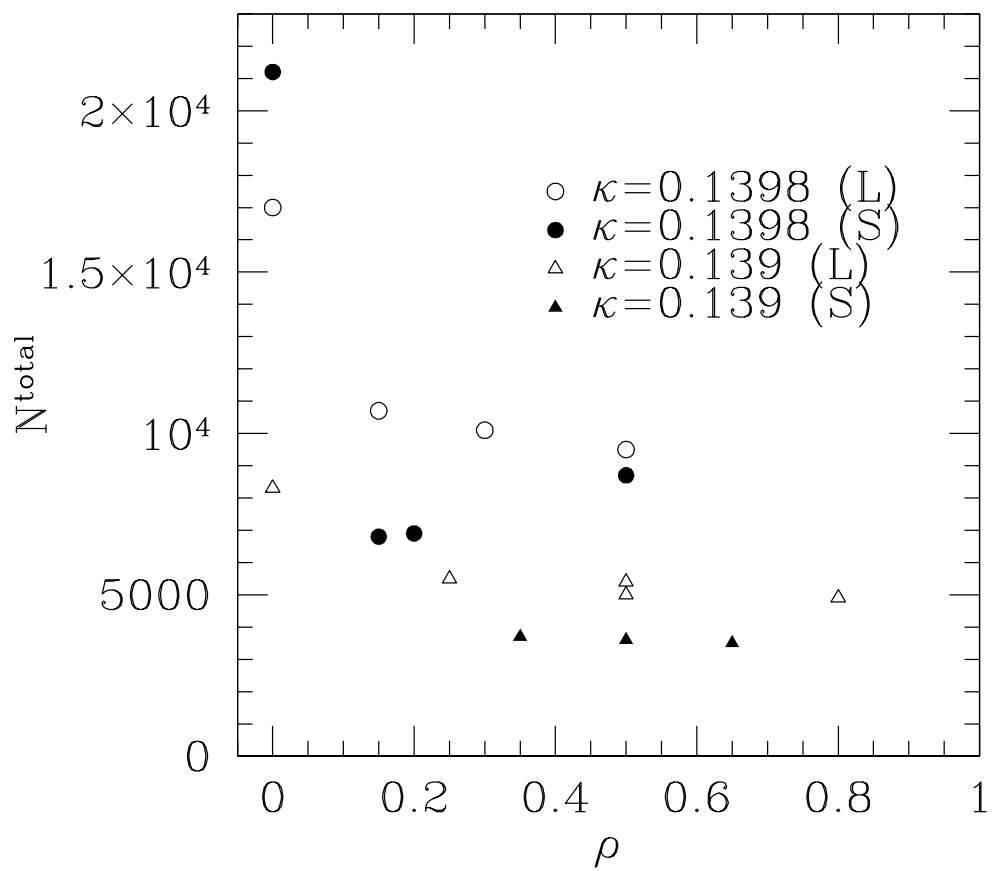


Figure 2: Performance results in terms of the total number of iterations N^{total} in the BiCGstab solver as a function of ρ . We denote by (L) the leap frog and by (S) the improved integration scheme.

a solid statement, comparing the two modified actions.

In table 7 we give results for the plaquette and for the maximal and minimal eigenvalues of \hat{Q}^2 . The numbers that are quoted are naive averages over all runs listed in table 5 and the runs with the action S_F in table 6. The error-bars are naively computed from the fluctuation of the averages of the single runs. Since the computation of the smallest and the largest eigenvalue of \hat{Q}^2 is rather CPU-consuming, we had measured it for $\kappa = 0.1390$ and $\kappa = 0.1398$ only once at the beginning of the run. For $\kappa = 0.1395$ we measured the eigenvalues after each trajectory. Our results for the plaquette for $\kappa = 0.1390$ and $\kappa = 0.1398$ are consistent within the quoted error-bars with those of [18]. In the case of $\kappa = 0.1395$ there is a 2σ discrepancy. The average value of λ_{max} is, within error-bars, identical for all three values of κ that we had studied. On the other hand, λ_{min} is decreasing as κ_c is approached. Fitting the three values with the ansatz

$$\lambda_{min} = C(\kappa_c - \kappa)^x \tag{57}$$

we obtain $x = 1.85 \pm 0.09$, where we have fixed $\kappa_c = 0.1405$.

5 Conclusion and outlook

In ref. [15] we suggested that the Hybrid-Monte-Carlo simulation of dynamical Wilson fermions can be substantially speeded up by a modification of the pseudo-fermion action. The basic idea is that the fermion matrix is split up into two factors such that each factor has a smaller condition number than the original fermion matrix. For each of the factors, a pseudo-fermion field is introduced. In ref. [15] we found a speed-up of more than a factor of two for the largest value of κ that we simulated.

In the present paper we have developed the idea of ref. [15] in a more general fashion. In addition to the original factorisation we discuss a second that is inspired [24] by twisted mass QCD [25]. Note that in our approach only one additional free parameter ρ appears as compared with the standard HMC simulations. Our numerical results show that no fine tuning of the parameter ρ is needed. We argued that the condition number for the modified fermions is changed to the square root of the original condition numbers. This bears the potential of changing the scaling behaviour of the HMC algorithm when the chiral limit is approached. We have also demonstrated that the modified pseudo-fermion action can be easily used on top of even-odd preconditioning of the clover-improved Wilson fermion matrix.

In our numerical study we find that for lattice-spacings, quark masses and lattice sizes that recently have been used in large scale simulations [18] a reduction of the numerical cost of more than a factor of two compared with the standard pseudo-fermion action can be achieved.

Table 5: Results for the $16^3 \times 24$ lattice at $\beta = 5.2$ and $c_{sw} = 1.76$ with the pseudo-fermion action S_F of eq. (20). For each set of parameters we have generated 100 trajectories, starting from an equilibrated configuration.

κ	scheme	ρ	R^2	$\delta\tau$	P_{acc}	N^{total}
0.139	L	0.	0.001	0.01	0.82(2)	8300
0.139	L	0.05	0.001	0.02	0.69(3)	6600
0.139	L	0.1	0.001	0.02	0.75(3)	6200
0.139	L	0.25	0.001	0.02	0.78(3)	5400
0.139	L	0.5	1.	0.02	0.12(3)	3200
0.139	L	0.5	0.1	0.02	0.68(4)	3700
0.139	L	0.5	0.01	0.02	0.77(2)	4500
0.139	L	0.5	0.001	0.02	0.81(2)	5000
0.139	L	0.8	0.001	0.02	0.77(2)	4900
0.139	L	1.2	0.001	0.02	0.69(3)	4100
0.139	S	0.1	0.0001	0.066...	0.61(3)	4400
0.139	S	0.2	0.0001	0.066...	0.75(3)	3970
0.139	S	0.35	0.0001	0.066...	0.78(2)	3700
0.139	S	0.5	0.0001	0.066...	0.80(3)	3600
0.139	S	0.65	0.0001	0.066...	0.76(2)	3500
0.139	S	0.8	0.0001	0.066...	0.68(3)	3400
0.139	S	1.0	0.0001	0.066...	0.60(3)	3500
0.1398	L	0.	0.0001	0.01	0.77(3)	17000
0.1398	L	0.05	0.0001	0.02	0.62(3)	11700
0.1398	L	0.15	0.0001	0.02	0.75(3)	10700
0.1398	L	0.3	0.0001	0.02	0.76(2)	10100
0.1398	L	0.5	0.1	0.02	0.53(4)	5800
0.1398	L	0.5	0.01	0.02	0.75(3)	7000
0.1398	L	0.5	0.0001	0.02	0.78(2)	9500
0.1398	L	1.0	0.0001	0.02	0.64(4)	9300
0.1398	S	0.	0.0001	0.02	0.64(4)	16500
0.1398	S	0.	0.0001	0.0166...	0.82(2)	21200
0.1398	S	0.05	0.0001	0.066...	0.35(4)	7500
0.1398	S	0.1	0.01	0.066...	0.46(4)	5100
0.1398	S	0.1	0.0001	0.066...	0.67(3)	6500
0.1398	S	0.15	0.0001	0.066...	0.72(3)	6800
0.1398	S	0.2	0.01	0.066...	0.60(3)	4700
0.1398	S	0.2	0.0001	0.066...	0.74(3)	6900
0.1398	S	0.4	0.0001	0.066...	0.49(3)	6100
0.1398	S	0.5	0.0001	0.04545 ...	0.82(2)	8700

Table 6: Results for the $16^3 \times 24$ lattice at $\kappa = 0.1395$. For the action of eq. (20) we have chosen $R^2 = 0.001$ as stopping criterion of the BiCGstab solver. In all cases, we have used the Sexton-Weingarten improved scheme. Each of the runs with the action of eq. (20) consists of 100 trajectories while the run with the action of eq. (21) consists of 380 trajectories. We have used a step-size of $\delta\tau = 0.057$ and 17 steps per trajectory. I.e. the trajectory length is not exactly equal to 1. In the case of the action eq. (20), we computed the acceptance rate P_{acc} by averaging $\min[1, \exp(-\Delta H)]$, while for the action of eq. (21) we just have counted the accepted configurations. N_1 and N_2 give the number of iterations needed by the solvers for the computation of the force due to S_{F1} and S_{F2} , respectively. Note that the BiCGstab has to be applied twice, while the CG is only applied once to compute the force.

action	ρ	$\delta\tau$	P_{acc}	N_1	N_2
20	0.05	0.066...	0.40(3)	30.2	70
20	0.2	0.066...	0.78(3)	15.4	67
20	0.5	0.066...	0.66(3)	9.2	61
21	0.2236	0.057	0.75(3)	31.25	223

Table 7: Results for the observables from the simulations of the $16^3 \times 24$ lattice. For comparison we give the result for plaquette obtained in ref. [18] (P_{UKQCD}). A discussion of the error-bars is given in the text.

κ	P_{UKQCD}	P	λ_{max}	λ_{min}
0.1390	0.51593(14)	0.51602(12)	2.95(2)	0.00110(4)
0.1395	0.52196(9)	0.52174(9)	2.960(4)	0.000513(7)
0.1398	0.52477(12)	0.52466(11)	2.95(2)	0.00028(2)

One interesting observation in our study is that the partially improved scheme of Sexton and Weingarten does profit more from the modification of the pseudo-fermion action than the leap-frog scheme. In fact, this is not too surprising, since higher order schemes have more problems in the limit $\kappa \rightarrow \kappa_c$ than the leap-frog scheme. This is nicely studied in [36] and also found in recent large scale simulations [11]. Based on our experience it would be interesting to study genuinely higher order integration schemes combined with the modified pseudo-fermion action.

There are a number of directions in which the present work could be extended. Our general framework (15) allows for a large variety of factorisations of the fermion matrix beyond our two choices of eqs. (20) and (21). For example, one could divide the lattice in sub-lattices and construct the matrix W by eliminating all hopping terms from \hat{Q} that connect different sub-lattices. Such a construction might be particularly useful for a massively parallel computer.

An obvious idea is to enlarge the number of factors in eq. (15). This might be particularly advantageous, when we go to light quark masses. In order to keep the condition number of the factors of the fermion matrix constant as the quark mass becomes lighter, more factors have to be introduced.

A related modification of the HMC algorithm has been proposed and tested in refs. [10, 43]. The first difference compared with our approach is the factorisation of the fermion matrix:

$$\tilde{M} = P(M)^{-1} \quad , \quad (58)$$

where $P(M)$ is a low order polynomial approximation of M^{-1} . The order of the polynomial plays a similar role as the parameter ρ in our approach. The use of the polynomial might allow for a better separation of the UV-part of the spectrum than our factorisation. On the other hand, the polynomial $P(M)$ requires the introduction of an auxiliary field for each order of the polynomial.

In contrast to us, the authors of ref. [10, 43] put the two contributions of the pseudo-fermion action on different time scales of the integration scheme. In our case it would also be possible to put S_{F1} on the same time scale as S_G . In fact, preparing ref. [15] we have tested this idea. However we found no advantage compared with our present setting. In order to keep the algorithm as simple as possible, we did not discuss this possibility here.

An interesting idea is to apply the idea of refs. [10, 43] to the Polynomial-Hybrid-Monte-Carlo algorithm [44, 45]. I.e. to use a polynomial approximation for both parts of the pseudo-fermion action:

$$S_{F1} = |P_1(M)\phi_1|^2 \quad , \quad S_{F2} = |P_2(M)\phi_2|^2 \quad , \quad (59)$$

where now $P_1(M)$ is a rough, low order approximation of M^{-1} and the product $P_1(M)P_2(M)$ is an accurate approximation of M^{-1} . This idea is particularly appealing since it could well be applied to the simulation of three flavour QCD. (See ref. [28] and refs. therein).

6 Acknowledgements

We thank R. Sommer for discussions. We are grateful to M. Lüscher who provided us with his benchmark code for the Dirac-operator. This work was supported in part by the European Community's Improving Human Potential Programme under contracts HPRN-CT-2000-00145 (Hadrons/Lattice QCD) and HPRN-CT-2002-00311 (EURIDICE).

References

- [1] T. Lippert, Nucl.Phys.B (Proc.Suppl.) 106&107 (2002) 193, hep-lat/0203009.
- [2] A. Ukawa, Nucl.Phys.B (Proc.Suppl.) 106&107 (2002) 195.
- [3] H. Wittig, Nucl.Phys.B (Proc.Suppl.) 106&107 (2002) 197, hep-lat/0203021.
- [4] C. Bernard et.al., Nucl.Phys.B (Proc.Suppl.) 106&107 (2002) 199.
- [5] F. Jegerlehner et al., CERN-2000-002 (1999).
- [6] V. Bernard, S. Hashimoto, D.B. Leinweber, P. Lepage, E. Pallante, S. R. Sharpe and H. Wittig, Panel discussion on chiral extrapolation of physical observables, (lattice2002), hep-lat/0209086.
- [7] S. Duane, A.D. Kennedy, B.J. Pendleton and D. Roweth, Phys.Lett.B 195 (1987) 216.
- [8] P. de Forcrand, Nucl.Phys.B (Proc.Suppl.) 47 (1996) 228, hep-lat/9509082.
- [9] K. Jansen, Nucl.Phys.B (Proc.Suppl.) 53 (1997) 127, hep-lat/9607051.
- [10] M. Peardon, Nucl.Phys.B (Proc.Suppl.) 106&107 (2002) 3, hep-lat/0201003.
- [11] CP-PACS Collaboration, A. Ali Khan et al., Phys.Rev.D 65 (2002) 054505, hep-lat/0105015.
- [12] UKQCD Collaboration, C.R. Allton et al., Phys.Rev.D 65 (2002) 054502, hep-lat/0107021.
- [13] A.C. Irving, Improved Wilson QCD simulations at light quark masses, (lattice 2002, QCD spectrum and quark masses), hep-lat/0208065.
- [14] CP-PACS Collaboration: Y.Namekawa et al., Exploring QCD at small sea quark masses with improved Wilson-type quarks, (lattice2002, spectrum), hep-lat/0209073.

- [15] M. Hasenbusch, Phys.Lett. B 519 (2001) 177, hep-lat/0107019.
- [16] M. Hasenbusch and K. Jansen, Nucl.Phys.B (Proc.Suppl.) 106&107 (2002) 1076, hep-lat/0110180.
- [17] B. Sheikholeslami and R. Wohlert, Nucl.Phys.B 259 (1985) 572.
- [18] Z. Sroczynski, Ph.D. thesis, Edinburgh (1998).
- [19] F. Knechtli, M. Della Morte, J. Rolf, R. Sommer, I. Wetzorke, U. Wolff, Running quark mass in two flavor QCD, (lattice2002, spectrum), hep-lat/0209025.
- [20] M. Hasenbusch and K. Jansen, Speeding up the HMC: QCD with Clover-Improved Wilson Fermions, (lattice 2002, algorithms), hep-lat/0210036.
- [21] M. Lüscher, S. Sint, R. Sommer, P. Weisz, U. Wolff, Nucl.Phys.B 491 (1997) 323, hep-lat/9609035.
- [22] K. Jansen and R. Sommer, Nucl.Phys.B 530 (1998) 185, hep-lat/9803017.
- [23] K. Jansen and C. Liu, Comput.Phys.Commun. 99 (1997) 221, hep-lat/9603008.
- [24] R. Sommer, private communication.
- [25] R. Frezzotti, P.A. Grassi, S. Sint and P. Weisz, JHEP 0108 (2001) 058, hep-lat/0101001.
- [26] K. Jansen, C. Liu, M. Lüscher, H. Simma, S. Sint, R. Sommer, P. Weisz, U. Wolff, Phys.Lett.B 372 (1996) 275, hep-lat/9512009.
- [27] X.Q. Luo, Comput. Phys. Commun. 94 (1996) 119, hep-lat/9603021.
- [28] JLQCD Collaboration: S. Aoki, R. Burkhalter, M. Fukugita, S. Hashimoto, K-I. Ishikawa, N. Ishizuka, Y. Iwasaki, K. Kanaya, T. Kaneko, Y. Kuramashi, M. Okawa, T. Onogi, S. Tominaga, N. Tsutsui, A. Ukawa, N. Yamada, T. Yoshié, Phys.Rev.D 65 (2002) 094507, hep-lat/0112051.
- [29] M.J. Peardon, Accelerating the Hybrid Monte Carlo algorithm with ILU preconditioning, hep-lat/0011080.
- [30] R. Frezzotti, M. Hasenbusch, J. Heitger, K. Jansen and U. Wolff, Comput.Phys.Commun. 136 (2001) 1, hep-lat/0009027.
- [31] P. de Forcrand and T. Takaishi, Nucl.Phys.B (Proc. Suppl.) 53 (1997) 968, hep-lat/9608093.

- [32] M. Hasenbusch, Phys.Rev.D 59 (1999) 054505, hep-lat/9807031.
- [33] J.C. Sexton and D.H. Weingarten, Nucl.Phys.B 380 (1992) 665.
- [34] M. Creutz and A. Gocksch, Phys.Rev.Lett 63 (1989) 9.
- [35] M. Campostrini and P. Rossi, Nucl.Phys.B 329 (1990) 753.
- [36] T. Takaishi, Comput.Phys.Commun. 133 (2000) 6, hep-lat/9909134.
- [37] B. Joó, B. Pendleton, A.D. Kennedy, A.C. Irving, J.C. Sexton, S.M.Pickles, S.P. Booth, Phys.Rev.D 62 (2000) 114501, hep-lat/0005023.
- [38] M. Lüscher, Nucl.Phys.B (Proc.Suppl.) 106&107 (2002) 21, hep-lat/0110007.
- [39] A. Frommer, V. Hannemann, Th. Lippert, B. Nöckel, K. Schilling, Int.J.Mod.Phys.C 5 (1994) 1073, hep-lat/9404013.
- [40] B. Joo, B. Pendleton, A.D. Kennedy, A.C. Irving, J.C. Sexton, S.M. Pickles, S.P. Booth, Phys.Rev.D 62 (2000) 114501, hep-lat/0005023.
- [41] C. Liu, A. Jaster and K. Jansen , Nucl.Phys.B 524 (1998) 603, hep-lat/9708017.
- [42] R.Frezzotti and K.Jansen, Nucl.Phys.B 555 (1999) 395, hep-lat/9808011; Nucl.Phys.B 555 (1999) 432, hep-lat/9808038.
- [43] M. Peardon and J. Sexton, Multiple molecular dynamics time-scales in Hybrid Monte Carlo fermion simulations, (Lattice2002, algorithms), hep-lat/0209037.
- [44] P. de Forcrand and T. Takaishi, Nucl.Phys.B (Proc. Suppl.) 53 (1997) 968, hep-lat/9608093.
- [45] R. Frezzotti and K. Jansen, Phys. Lett. B 402 (1997) 328, hep-lat/9702016.